Supplementary Materials

Sample Preparation, Experimental and Analytical Methods

Sample preparation

Olivine grains, 150-850 μm diameter and containing MIs, were handpicked from 7 samples (10020,49, 12008,5, 12040,199, 15016,22, 15647,22, 74220,871, and 74235,22). We also examined lunar soil 15421,22 (containing high proportion of green glass beads) but no olivine crystals with MIs more than a few μm diameter were found. Individual loose plagioclase crystals with glassy MIs have been identified in 15421,22 and examined, but the inclusions are too small (≤ 7 μm diameter) to be located accurately for SIMS analyses.

Olivine-hosted MIs in 74220,871 (containing high proportion of orange glass beads) are naturally glassy or nearly glassy. All other olivine-hosted MIs are crystalline (one inclusion in 10020 is partially glassy). Some crystalline MIs from 10020, 12008, and 15016 were homogenized at 1540K (see below) prior to microbeam analyses, and some were analyzed using a large-sized beam without homogenization. Because volatile components (H_2O, F, S, Cl) and non-volatile elements are analyzed in different SIMS sessions, for the unhomogenized crystalline inclusions, the volatile analyses and non-volatile elemental analyses are not on the same material and are hence not directly comparable. Only glassy (including the naturally glassy and homogenized) MIs are used for quantitative purposes.

Olivine grains containing MIs (some after homogenization) are prepared into thin wafers, with MI exposed on the top surface. Before and during sample preparation, the MIs were carefully examined under optical microscope to ensure they are not connected to cracks. The samples were mounted in indium metal following previous studies (e.g., Hauri et al. 2002). Major elements of these samples were analyzed by Electron Microprobe Analyzer (EMPA) at the University of Michigan. Volatiles were analyzed by Secondary Ion Mass Spectrometry (SIMS and NanoSIMS) at Caltech. Nonvolatile trace elements were analyzed separately by SIMS at Caltech after the analyses of volatile elements.

Two glass beads, each from 74220,871 (orange glass) and 15421,22 (green glass), were also polished and analyzed for major, volatile, and nonvolatile trace elements.

Homogenization experiments

Micro-beam analysis on the crystalline MIs may yield biased results due to the chemical heterogeneity at micrometer to ten-micrometer scale. In order to avoid this effect, some crystalline MIs were homogenized into glassy inclusions by melting at high temperatures before polish and chemical analysis.

Homogenization experiments were carried out in a Deltech vertical gas-mixing furnace at the University of Michigan. Olivine crystals with crystalline MIs were placed in graphite crucibles and then placed inside the Deltech furnace but initially far away from the hot spot. The furnace was first set to about 1540 K under high-purity N_2 gas environment at one bar pressure. The temperature was chosen to be slightly higher than the dry liquidus temperature of the lunar basalts at one bar, such that the MIs would become completely molten at this temperature. High-purity N_2 gas (99.9999% with less than 0.15 ppm of moisture and O_2, 0.10 ppm of total hydrocarbons and $CO+CO_2$) was used to protect the olivine crystals and graphite crucibles from being oxidized, and to prevent any possible terrestrial water contamination into the MIs during the experiments. Specifically, we decided not to use piston-cylinder experiments to homogenize the crystalline MIs to avoid any possible addition of terrestrial water. In one-atmosphere water-free experiments, there is no likelihood of gaining water.

Once the desired temperature is reached, the graphite crucible with olivine grains was slowly inserted to the hot spot of the furnace (in ≤ 10 minutes), and held at 1540 K for 2 minutes. Such short homogenization duration is chosen to be just enough to melt the inclusion based on trial and error, so as to avoid possible water loss from MIs. The graphite crucibles were then rapidly taken out and half-

submerged in water to quench. The olivine crystals were quenched in less than one minute. During quench, water was kept out of the crucibles to prevent olivine cracking and water contamination.

At least two processes during homogenization might have affected the composition of the melt inclusions. One is the inward dissolution or crystallization of the olivine host into the MI depending on the MgO content of the homogenized melt inclusion. The majority of the homogenized melt inclusions and the host olivine have Fe/Mg exchange coefficient of 0.30±0.03, suggesting rough equilibrium. The equilibrium could be the initial state or could have been reached during the homogenization experiment due to host olivine dissolution or crystallization into the MI. That is, if there was post-entrapment inward crystallization of olivine, the homogenization experiment re-established the equilibrium. Some MIs have higher MgO than the expected equilibrium concentration with the host olivine. This might be due to insufficient time to homogenize the melt inclusion (e.g., grains with low MgO have not melted). Another effect is possible water loss from the MI by diffusion through the olivine host. Based on model calculation (Chen et al. 2013), less than 1% of the total dissolved water in the MIs would be lost during the short duration of heating. Even though we have taken various precaution steps and it is unlikely that H_2O would be lost from the MIs during homogenization, we cannot completely rule out the possibility of water loss; e.g., there might be microcracks or nanocracks along which H_2O could be lost during short-duration heating.

Electron microprobe analyses of major elements

Major elements were analyzed by a Cameca SX100 electron microprobe at the University of Michigan, using 15 kV acceleration voltage, 5 nA current, and 10 μm scanning beam. For crystalline MIs, multiple spots were analyzed and averaged for each inclusion to better represent the whole inclusion composition.

SIMS analyses of volatiles

Volatiles (H analyzed as OH and reported as H_2O, F, S, and Cl) were analyzed in five SIMS analysis sessions at Caltech, two on a Cameca NanoSIMS 50L, and the other three sessions on a Cameca IMS 7f-GEO. We generally followed previous analytical procedures (e.g., Hauri et al. 2002, Mosenfelder et al. 2011), with efforts particularly aimed to reduce the hydrogen background during analyses. Samples were stored in a vacuum oven at about 70 ºC for a few days before being placed in the high vacuum chamber of the SIMS instruments. When possible, samples were held in the high vacuum chamber over weekend before analysis. The instruments were baked for one day before the analysis sessions. For the IMS 7f-GEO, a liquid N_2 cold trap was also used to improve the vacuum condition. The vacuum in the sample chamber was about 6×10^{-10} torr for the NanoSIMS 50L, and about 1.5×10^{-10} torr for the IMS 7f-GEO.

Seven MPI-Ding glasses (GOR128-G, GOR132-G, KL2-G, ML3B-G, StHs6/80-G, T1-G, ATHO-G) (Jochum et al. 2000, 2006) plus a mid-ocean ridge basalt (MORB) glass were used as standards. The water concentrations in the reference glasses were analyzed by FTIR at the University of Michigan. F, S, and Cl concentrations in the MPI-Ding glasses were from Jochum et al. (2006). S concentration in the MORB glass was analyzed by EMPA. F and Cl concentrations in the MORB glass were not determined. A dry olivine standard (GRR1017) was used to examine the background of the ion species.

For the analytical sessions using NanoSIMS 50L, seven ion species, ^{12}C, $^{16}O^{1}H$, ^{18}O, ^{19}F, ^{30}Si, ^{32}S, and ^{35}Cl, were generated using a 0.5-1 nA and 5 μm diameter Cs^+ primary ion beam and simultaneously analyzed by seven electron multiplier detectors. In one analysis session, ^{30}Si was replaced by ^{31}P, in order to confirm that the analysis spot was completely within the MIs by comparing the P concentrations by SIMS and EMPA methods. Sample charging was compensated by an electron gun. The best analysis position of the MI was verified by the contrasting secondary ion signals between the inclusion and host olivine. Each analysis position was pre-sputtered by the primary ion beam rastered over a 10×10 μm area. The primary ion beam then rastered over the center 5×5 mm area, and secondary ions from the center 3×3 μm area (electronic gating) were counted for 3.6 minutes. ^{18}O counting rate was on the order of 1×10^{5} counts per second, and $^{16}O^{1}H/^{18}O$ on a dry olivine standard was about 2×10^{-3}.

For the analytical sessions using IMS 7f-GEO, the same seven ion species were analyzed with a particular focus to obtain low H_2O detection limit. A 2-5 nA and 15 μm diameter Cs^+ primary ion beam was used to generate the negative ions, which were then sequentially analyzed by an electron multiplier detector. Sample charging were compensated by an electron gun. A mass resolving power of ~5000 was used to separate $^{16}O^1H$ from ^{17}O. Each analysis position was pre-sputtered by the primary beam rastering over a 25×25 μm area for 2 minutes. For data collection, the primary ion beam rastered the center 10×10 μm area, and secondary ions from the center 8×8 μm area were counted. Automatic peak centering and mass calibration were performed during the analyses. In each counting cycle, the counting time was 2 seconds for ^{12}C, and 1 second for the others. Each analysis position was analyzed for 20 cycles. ^{18}O counting rate was about the same as that of the NanoSIMS, but $^{16}O^1H/^{18}O$ on a dry olivine standard was about 3×10^{-4}, nearly one order of magnitude smaller than that of the NanoSIMS.

Volatiles: SIMS data processing

Many MIs were repeatedly analyzed by SIMS in each session as well as in different sessions, in order to examine reproducibility and to obtain good average volatile concentrations representing the whole inclusions. Glassy MIs generally yielded consistent data across different analysis points. Crystalline MIs showed much larger scatters than the glassy ones, as expected from heterogeneity of such inclusions. Data were examined and filtered based on the following three criteria: (1) Each analysis position was examined under optical microscope and Scanning Electron Microscopy (SEM) at the University of Michigan after SIMS analysis, and data on problematic positions were excluded; (2) Data with low ^{30}Si or ^{18}O counting rate were rejected, because they indicate possible misalignment of the secondary ion beam; (3) Data with high ^{12}C counting rate were generally rejected, because they may contain surface/crack contamination signals. $^{12}C/^{18}O$ background was about 2×10^{-4} in the NanoSIMS, and 4×10^{-5} in the 7f-GEO. Some data show high ^{12}C counts, but their H_2O concentrations are consistent with those with low ^{12}C counts. Because tiny residual carbon coating from prior electron microprobe analyses can lead to large C signals, these H_2O data were kept. High ^{12}C counts were not found to correlate with high F, S, or Cl concentrations.

Calibration lines for each SIMS session were established using the glassy standards. Two different calibrations were established for basaltic composition and andesitic-dacitic composition. Fig. 1 shows some examples of calibration curves. For the NanoSIMS data, relative uncertainties are 5% for H_2O, 11% for F and S, and 6% for Cl, based on the reproducibility of the glass standards. The detection limits are 15 ppm for H_2O, 0.01 ppm for F, 0.2 ppm for S, and 0.1 ppm for Cl. For the 7f-GEO data, relative uncertainties are 12% for H_2O and F, 13% for S, and 8% for Cl, and the detection limits are 1 ppm for H_2O, 0.01 ppm for F, 0.3 ppm for S, and 0.03 ppm for Cl.

SIMS analyses of trace elements

Twenty trace elements (Sr, Y, Zr, Nb, Ba, La, Ce, Pr, Nd, Sm, Eu, Gd, Tb, Dy, Ho, Er, Tm, Yb, Lu, Hf) were analyzed with Cameca IMF 7f-GEO at Caltech, using the energy-filtering technique (e.g., Zinner and Crozaz, 1986). In one SIMS session, Al, K, and U were also analyzed. The Al concentration is compared to their concentrations by EMPA method, in order to confirm that the SIMS spots were completely within the MIs. The analyzed concentration of Al or Sr (one of the best analyzed trace element) should be close to, or slightly higher than the respective concentration in the glass beads or whole rock (http://curator.jsc.nasa.gov/Lunar/lsc/index.cfm) due to post-entrapment crystallization. Hence, we use the criterion that if the Al concentration is lower than that in the glass beads by more than 10%, or if the Sr concentration is lower than that in the glass beads or whole rock by more than 20% (the 10% and 20% are used to allow for analytical errors), then the trace element data are considered to have been diluted by beam overlapping with or drilling into olivine, and are discarded. In this way, we prevent the volatile to refractory elemental ratios from being too high.

Positive ions of ^{30}Si and the above trace elements were generated by a 5-15 nA and 15 μm diameter O^- primary ion beam. Each analysis position was pre-sputtered by the primary beam rastering over a 20×20 μm area for 10-30 seconds. The short pre-sputtering time was sufficient because trace elements

analyses were always on previous analysis positions of volatiles. The secondary ion beam and the peak position of ^{30}Si were then automatically centered. During analyses, the primary ion beam rastered the center 10×10 μm area, and secondary ions from this area were counted (no electronic gating). In each counting cycle, the counting time was 1 s for ^{30}Si, and 2-10 s for the trace element ions. Each analysis position was analyzed for 6 cycles.

Two glass standards from the National Institute of Standards and Technology (NBS610 and NBS612) (Gladney et al., 1987) and an MPI-Ding glass (T1-G) (Jochum et al., 2006) were used as trace elements standards. 2σ relative uncertainties are 10% or less for Sr, Y, Zr, Ba, Ce, Nd, and Dy, 10-30% for Nb, La, Pr, Sm, Gd, Tb, Ho, Er, Yb, and U, about 50% for Tm and Lu, and 100-200% for Eu and Hf.

EMPA and SIMS analyses of the unhomogenized crystalline MIs vs. homogenized MIs

Initially we thought that good data could be obtained on unhomogenized crystalline MIs by using a large beam size to sample a large area. Hence, data were collected on the unhomogenized crystalline MIs (Table S4). Eventually we decided that the practice is not optimal: because we need to examine the systematic correlation between volatile and nonvolatile elements, but different grains inside an unhomogenized crystalline melt inclusion can have difference ratios. In addition, volatile elements and nonvolatile elements are measured in different sessions and hence sampled different volumes, leading to even larger variation in the volatile to nonvolatile elemental ratios. Specifically, a high volatile to non-volatile elemental ratio may be artifact of the analyses. Hence, the data on the unhomogenized crystalline melt inclusions are not used to estimate lunar volatiles concentrations in the lunar mantle.

When the homogenized MIs are compared with the unhomogenized crystalline MIs, on average, they have similar average concentrations but the unhomogenized MIs are more scattered in concentrations. For example, H_2O concentrations in the homogenized MIs range from 5 to 131 ppm, and those in the unhomogenized crystalline MIs range from 2 to 336 ppm. The homogenized MIs contain 22-117 ppm F, 0.1-6.0 ppm Cl, and 363-1990 ppm S, whereas the unhomogenized crystalline MIs contain 20-513 ppm F, 0-19 ppm Cl, and 21-1794 ppm S. The larger scatter in elemental concentrations in the unhomogenized MIs compared to the homogenized MIs is expected because even a large beam size is used, an analysis on an unhomogenized MI samples a small region of a heterogeneous MI. The similar average concentrations between unhomogenized and homogenized MIs imply that H_2O and other volatile loss during the short-duration homogenization is probably minimal, although we cannot rule it out.

H_2O by FTIR

Water concentrations in the SIMS standards and selected MIs were analyzed by a microscope system of a PerkinElmer GX FTIR spectrometer at the University of Michigan. Olivine crystals containing large and glassy MIs were taken out from indium mount after SIMS analysis and doubly polished to expose the inclusions on both top and bottom surfaces. Some MIs were lost in this process. Good IR spectra were obtained for only one melt inclusion although many were measured. The absorbance at 3500 cm^{-1} wavenumber was measured using a straight baseline correction. Water concentration was calculated using the Beer-Lambert law (e.g., Stolper 1982).

Rarity of amphibole in lunar rocks

If the primitive lunar mantle contains ~100 ppm H_2O, then why are hydrous minerals such as amphibole are so rare in lunar rocks (McCubbin, 2007)? We focus here on amphibole because it is the most common igneous hydrous mineral in terrestrial mafic rocks. Mid-ocean ridge gabbros often contain primary igneous amphibole (e.g., Alt and Anderson, 1991; Coogan et al., 2001).

One important factor is that the lunar surface is essentially a vacuum, and the lithostatic pressure gradient on the moon is ~1/6 that on earth, so near-surface magmas likely degas extensively and are unable to crystallize amphibole (or other hydrous minerals). For example, 20 m depth of magma or rock is necessary to produce a pressure of 1 bar (the earth's surface pressure), and the solubility of H_2O in basalt at such a pressure is about 700 ppm (Liu et al., 2005; Newcombe et al., 2012). For measured H_2O content of 1400 ppm and CO_2 content of 6 ppm (Hauri et al., 2011), the vapor pressure of H_2O, H_2, CO_2, and CO would be 0.4, 1.0, 1.2, and 9.2 MPa at a logfO2 of IW–1(Newcombe et al., 2012), and the total

pressure would correspond to a magma depth of 2.4 km. Based on our conclusions above, lunar mafic magma is expected to contain similar or just slightly lower amount of H_2O as MORB, and to reach the right condition for amphibole growth if the pressure of crystallization is sufficient. Nicholis and Rutherford (2004) determined experimentally that the lowest H_2O pressure to stabilize F-free and Cl-free amphibole in basalt is 90 MPa, which is equivalent to 18 km depth in the moon (more than 18 km depth if the likely presence of other gases is considered), but only ≥2.4 km below the seafloor on the earth (assuming seafloor pressure of 25 MPa). Amphibole crystals in mid-ocean ridge gabbros are almost F-free and Cl-free; e.g., F+Cl in primary igneous amphibole crystals in mid-ocean ridge gabbros occupies less than 10% of the F+Cl+OH site (Coogan et al., 2001). Hence, the use of the results by Nicholis and Rutherford (2004) is appropriate. On the earth, gabbros from a depth of several km can be uplifted to near surface, e.g., along fracture zones. However, on the moon, excavating plutonic mafic rocks from ≥ 18 km depth is less likely. Nevertheless, some lunar highland breccias contain rocks that were inferred to come from 12 to 34 km depth (Herzberg and Baker, 1980) but are amphibole-free. We conclude that the absence of hydrous minerals in lunar rocks likely reflects the combined influences of degassing in a high-vacuum environment on the surface, combined with the great pressure required to stabilize amphibole in basaltic magmas of moderate water content, and the difficulty of sampling lunar rocks from great depth. Finally, it is worth noting that on the earth's surface, many hydrous minerals form due to weathering, diagenesis and metamorphism in the presence of liquid water, which is apparently lacking on the moon.

Another hydrous mineral that is often discussed in the context of lunar volatiles is apatite. Apatite is common in terrestrial basalts but much less common in lunar basalts. On the other hand, merrillite (previously often referred to as "whitlockite" or "lunar whitlockite", see Jolliff et al., 2006 for terminology) is more common in lunar basalts. Although in earlier years, the presence or absence of certain phosphate minerals were used to indicate wet or dry magmas and to infer H_2O concentrations (e.g., Boyce et al., 2010; Patino-Douce et al., 2011), more recent studies (Boyce et al., 2014; McCubbin et al., 2014; Pernet-Fisher et al., 2014), appear to reach the tentative conclusion that the occurrence or absence of specific phosphate minerals does not provide a strong constraint on H_2O content in lunar magmas because late-stage evolution of lunar basaltic magma can be very different from terrestrial basaltic magma.

References for the Supplementary Materials

Alt, J.C., Anderson, T.F., 1991. Mineralogy and isotopic composition of sulfur in layer 3 gabbros from the Indian Ocean Hole 735B. Proc. ODP Sci. Results 118, 113-125.

Coogan, L.A., Wilson, R.N., Gills, K.M., MacLeod, C.J., 2001. Near-solidus evolution of oceanic gabbros: insight from amphibole geochemistry. Geochim. Cosmochim. Acta 65, 4339-4357.

Gladney, E.S., O'Malley, B.T., Roelandts, I., Gills, T.E., 1987. Standard Reference Materials: Compilation of elemental concentration data for NBS clinical, biological, geological and environmental standard reference materials.

Hauri, E., Wang, J., Dixon, J.E., King, P.L., Mandeville, C., Newman, S., 2002. SIMS analysis of volatiles in silicate glasses 1. calibration, matrix effects and comparison with FTIR. Chem. Geol. 183, 99-114.

Herzberg, C.T., Baker, M.B., 1980. The corierite- to spinel-cataclasite transition: structure of the lunar crust, in: Papike, J.J., Merrill, R.B. (Eds.), Proc. Conf. Lunar. Highlands Crust, pp. 113-132.

Jochum, K.P., Dingwell, D.B., Rocholl, A., Stoll, B., Hofmann, A.W., Becker, S., Besmehn, A., Bessette, D., Dietze, H.J., Dulski, P., Erzinger, J., Hellerbrand, E., Hoppe, P., Horn, I., Janssens, K., Jenner, G.A., Klein, M., McDonough, W.F., Maetz, M., Mezger, K., Munker, C., Nikogosian, I.K., Pickhardt, C., PRaczek, I., Rhede, D., Seufert, H.M., Simakin, S.G., Sobolev, A.V., Spettel, B., Straub, S., Vincze, L., Wallianos, A., Weckwerth, G., Weyer, S., Wolf, D., Zimmer, M., 2000. The preparation and preliminary characterization of eight geological MPI-DING reference glasses for in-sity

923 microanalysis. Geostandards News. 24, 87-133.
924 Jochum, K.P., Stoll, B., Herwig, K., Willbold, M., Hofmann, A.W., Amini, M., Aarburg, S., Abouchami,
925 W., Hellebrand, E., Mocek, B., Raczek, I., Stracke, A., Alard, O., Bouman, C., Becker, S., Ducking,
926 M., Bratz, H., Klemd, R., de Briuin, D., Canil, D., Cornell, D., de Hoog, J., Dalpe, C., Danyushevsky,
927 L., Eisenhauer, A., Gao, Y., Snow, J.E., Groschopf, N., Gunther, D., Latkoczy, C., Guillong, M.,
928 Hauri, E.H., Hofer, H.E., etc., 2006. MPI-DING reference glasses for in situ microanalysis: new
929 reference values for element concentrations and isotope ratios. Geochem. Geophys. Geosys. 7,
930 Q02008, doi:02010.01029/02005GC001060.
931 Liu, Y., Zhang, Y., Behrens, H., 2005. Solubility of H_2O in rhyolitic melts at low pressures and a new
932 empirical model for mixed H_2O-CO_2 solubility in rhyolitic melts. J. Volcanol. Geotherm. Res. 143,
933 219-235.
934 McCubbin, F.M., Nekvasil, H., Lindsley, D.H., 2007. Is there evidence for water in lunar magmatic
935 minerals? A crystal chemical investigation. Lunar Planet. Sci. 38, abstract 1354.
936 Mosenfelder, J.L., Le Voyer, M., Rossman, G.R., Guan, Y., Bell, D.R., Asimow, P.D., Eiler, J.M., 2011.
937 Analysis of hydrogen in olivine by SIMS: evaluation of standards and protocol. Am. Mineral. 96,
938 1725-1741.
939 Newcombe, M.E., Brett, A., Beckett, J.R., Baker, M.B., Newman, S., Stolper, E.M., 2012. Solubility and
940 diffusivity of water in basic silicate melts at low pH_2O. AGU abstract and poster.
941 Nicholis, M.G., Rutherford, M.J., 2004. Experimental constraints on magma ascent rate for the Crater Flat
942 volcanic zone hawaiite. Geology 32, 489-492.
943 Stolper, E.M., 1982. Water in silicate glasses: an infrared spectroscopic study. Contrib. Mineral. Petrol.
944 81, 1-17.
945 Zinner, E., Crozaz, G., 1986. A method for the quantitative measurement of rare earth elements in the ion
946 microprobe. Int. J. Mass Spec. Ion Proc. 69, 17-38.
947

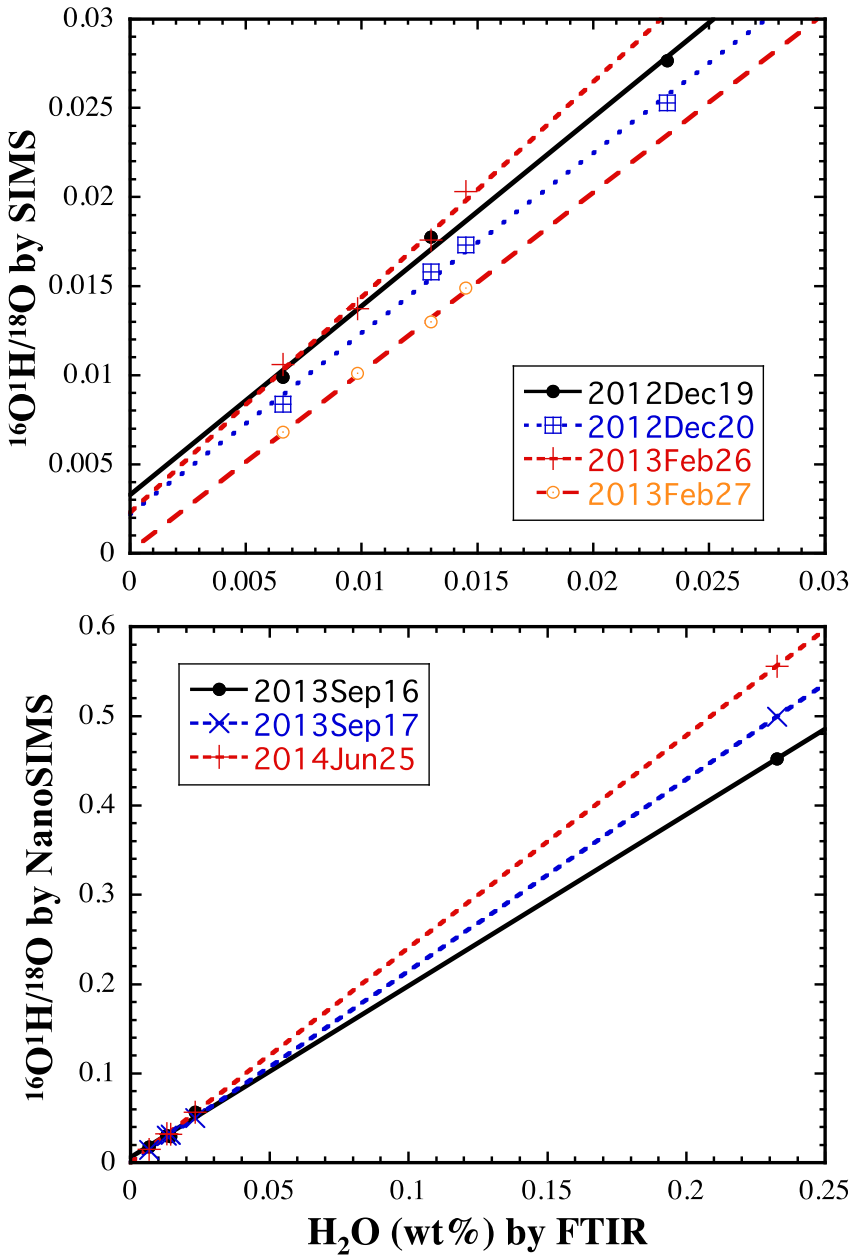

948
949
950 Fig. S1. Examples of calibration curves for the SIMS measurement of H_2O concentrations.
951

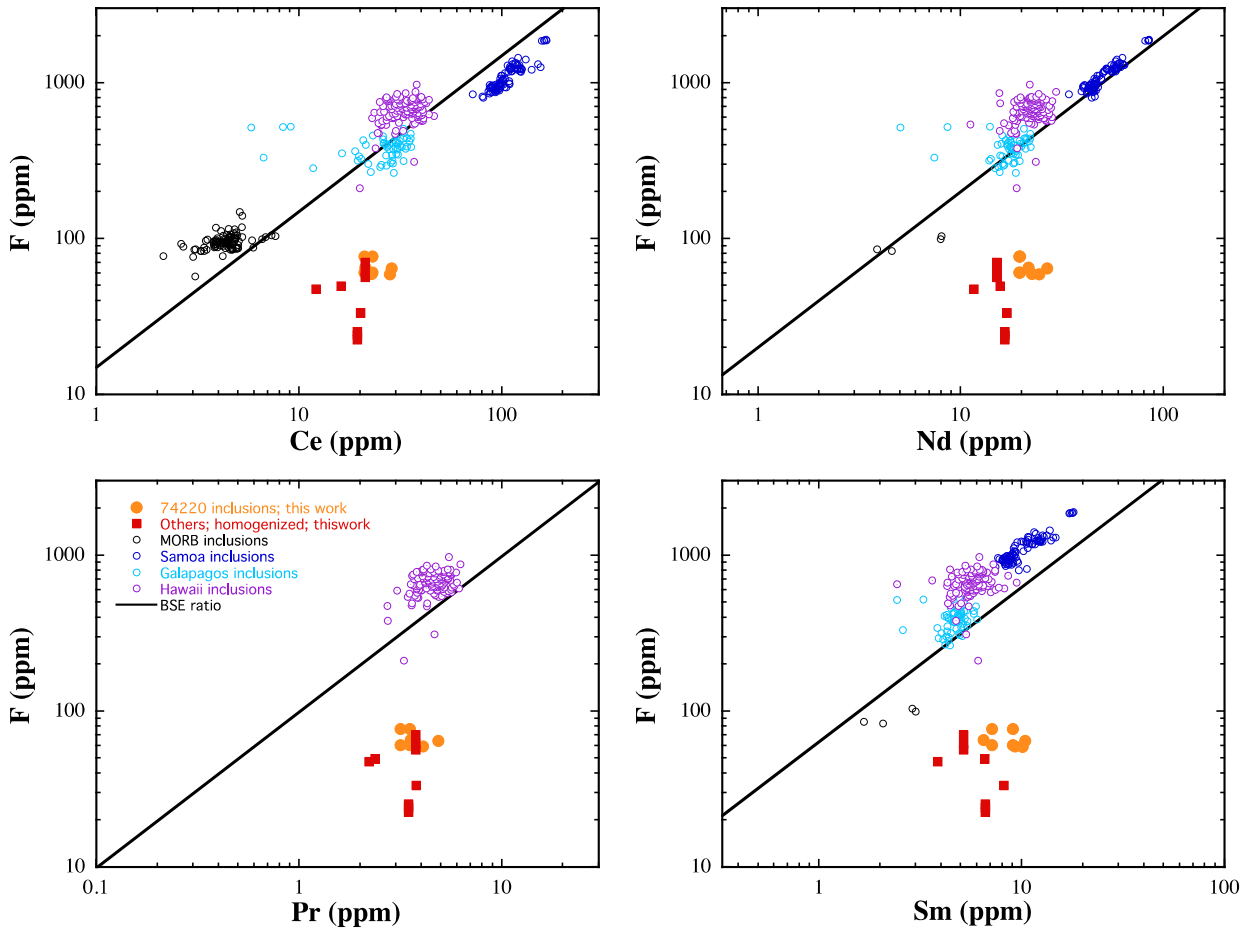

Fig. S1. F concentrations against La, Ce, Pr and Nd in olivine-hosted basaltic melt inclusions to examine the degree of incompatibility of F. Data sources are the same as in Fig. 4. The solid line is the elemental ratio from McDonough and Sun (1995). Best log-linear relation that is consistent with the BSE ratio is between F and Nd.

959 Table S1. Naturally glassy melt inclusions

Lunar sample #	74220								
MI #	1	3	5	8a	8b	9a	9a-2	12	14a
host olivine diameter (μm)	333	278	369	383	383	389	389	255	469
host olivine Fo#	80	81	80	80	81	78	78	74	
inclusion diameter (μm)	23	30	14	33	18	54	54	19	11
SiO_2 (wt%)	40.62	41.57		40.77	40.39	39.26		54.00	41.83
TiO_2	11.81	9.26		11.34	12.41	9.82		3.59	10.35
Al_2O_3	8.54	9.25		9.28	9.11	8.15		13.59	9.48
FeO	21.53	20.49		20.27	21.16	24.09		5.65	19.41
MnO	0.30	0.21		0.23	0.27	0.27		0.12	
MgO	3.74	4.75		3.64	4.20	5.37		1.95	7.48
CaO	11.35	11.53		12.01	11.05	9.89		18.97	9.81
Na_2O	0.46	0.54		0.500	0.56	0.38		0.64	0.72
K_2O	0.08	0.08		0.105	0.10	0.07		0.11	
P_2O_5	0.04	0.10		0.08	0.07	0.04		0.10	
Cr_2O_3				0.25	0.44	0.58		0.13	
H_2O (ppm)	574	802	661	860		1166	1097		671
F	34	57	57	59		77	60		48
S	391	731	541			691			803
Cl	1.71	2.3	2.2	3.3		2.8	3.8		3.0
Sr				313		245	280		
Y				55		53	54		
Zr				243		203	207		
Nb				27		17.7	21		
Ba				122		83	94		
La				8.1		6.6	6.9		
Ce				23		21	23		
Pr				4.1		3.5	3.2		
Nd				22		20	19.4		
Sm				9.3		7.1	9.0		
Eu				3.6		2.6	1.9		
Gd				9.7		9.6	9.6		
Tb				1.24		1.54	2.0		
Dy				10.2		10.4	9.5		
Ho				2.2		1.64	1.20		
Er				5.5		5.1	4.7		
Tm				0.47		0.59	0.48		
Yb				4.8		4.7	4.6		
Lu				1.0		0.68	0.22		
Hf				4.2		4.7	6.9		
U							0.089		

960

961

962 Table S1.

Lunar sample #	74220				10020			
MI #	14b	15a	15b	15c	11b	11b	11b	11b
host olivine diameter (μm)	469	339	339	339	188	188	188	188
host olivine Fo#					69	69	69	69
inclusion diameter (μm)	9	35	21	21	14	14	14	14
SiO_2 (wt%)	39.67	45.23	37.71	43.07	54.96			
TiO_2	8.33	9.12	11.40	9.12	4.64			
Al_2O_3	8.43	9.59	7.69	9.38	10.65			
FeO	21.44	18.94	23.29	19.96	7.41			
MnO			0.50		0.10			
MgO	9.70	5.25	5.15	4.65	2.34			
CaO	10.65	11.27	11.38	12.11	19.23			
Na_2O	0.54	0.72	0.45	0.54	0.68			
K_2O					0.18			
P_2O_5					0.11			
H_2O (ppm)	670	733	787	811		326		346
F	46	59	65	64	122	163	138	160
S	629	749	828	822	276	236	432	185
Cl	2.5	3.9	3.8	3.9	5.0	6.9	4.9	5.8
Sr		314	323	349	188			
Y		60	58	69	158			
Zr		244	221	282	399			
Nb		28	27	29	25			
Ba		118	112	122	141			
La		8.6	7.1	8.5	16.0			
Ce		28	21	29	49			
Pr		3.8	3.6	4.9	10.3			
Nd		24	22	27	46			
Sm		10.1	6.5	10.4	20			
Eu		5.9	6.7	2.9	0.34			
Gd		8.5	9.3	12.1	22			
Tb		1.47	1.51	1.47	3.6			
Dy		10.7	10.3	12.3	28			
Ho		2.4	2.1	1.93	7.0			
Er		4.1	5.9	6.1	16.7			
Tm		0.87	0.40	1.3	3.2			
Yb		4.7	5.8	5.5	19.9			
Lu		1.3	0.72	1.1	1.8			
Hf		11	0.22	11	14			
U		3.8		3.8				

963

964

965 Table S2. Homogenized melt inclusions

Lunar sample #	10020	12008						
MI #	16	2a	2a	2b	3	3	3	3
host olivine diameter (μm)	364	455	455	455	718	718	718	718
host olivine Fo#	70	70	70	70	76	76	76	76
inclusion diameter (μm)	83	46	46	25	74	74	74	74
SiO_2 (wt%)	39.22	41.20		47.01	44.75			
TiO_2	11.46	6.36		5.13	4.92			
Al_2O_3	10.49	8.39		11.10	10.18			
FeO	18.08	21.87		18.67	16.43			
MnO	0.31	0.24		0.18	0.27			
MgO	6.54	7.77		7.17	9.85			
CaO	11.33	10.28		11.47	11.39			
Na_2O	0.30	0.45		0.33	0.38			
K_2O	0.12	0.09		0.07	0.12			
P_2O_5	0.00	0.15		0.06	0.19			
H_2O (ppm)	131	31	5.4	5.2		4.7	77	22
F	49	117	113	32	56	76	62	70
S	1189	1990	974	512	428	644	480	1083
Cl	3.5	4.8	4.0	1.35	4.7	9.8	5.9	6.0
Sr	120				130			
Y	71				54			
Zr	162				162			
Nb	14.2				10.2			
Ba	45				77			
La	4.1				8.2			
Ce	16.1				21			
Pr	2.4				3.8			
Nd	15.6				15.1			
Sm	6.6				5.2			
Eu	0.78				2.0			
Gd	11.0				7.5			
Tb	2.1				1.56			
Dy	12.6				9.1			
Ho	2.9				3.1			
Er	7.6				6.3			
Tm	1.2				0.87			
Yb	8.7				5.9			
Lu	1.3				1.0			
Hf	7.6				4.7			
H_2O by FTIR (ppm)	95±33							

966

967

968 Table S2.

Lunar sample #	12008						15016
MI #	4a	4a	4a	4a	4b	4c	4
host olivine diameter (μm)	209	209	209	209	199	199	495
host olivine Fo#	68	68	68	68	68	68	57
inclusion diameter (μm)	29	29	29	29	25	28	44
SiO_2 (wt%)	48.95				44.42	42.41	47.58
TiO_2	5.47				5.95	5.41	2.70
Al_2O_3	10.15				11.39	10.49	10.03
FeO	11.23				12.83	18.94	14.71
MnO	0.37				0.26	0.24	0.28
MgO	10.66				7.89	6.77	9.37
CaO	11.75				12.40	11.60	10.53
Na_2O	0.45				0.52	0.31	1.82
K_2O	0.12				0.10	0.07	0.19
P_2O_5	0.16					0.16	0.02
H_2O (ppm)	58	2.9	38	21		22	54
F	23	27	24	25	33	47	25
S	391	447	423	633	916	1351	363
Cl	0.099	0.107	0.119	0.193	5.5	2.2	0.190
Sr	132				136	116	
Y	52				59	36	
Zr	140				150	98	
Nb	6.8				5.7	4.1	
Ba	56				62	47	
La	5.6				6.4	4.5	
Ce	19.4				20	12.1	
Pr	3.5				3.8	2.2	
Nd	16.5				16.9	11.6	
Sm	6.6				8.2	3.9	
Eu	1.7				2.1	1.7	
Gd	7.3				7.1	7.8	
Tb	1.35				1.55	1.34	
Dy	9.4				10.4	7.8	
Ho	1.97				2.9	1.19	
Er	6.1				6.9	4.4	
Tm	0.65				1.0	0.78	
Yb	6.6				6.4	4.3	
Lu	0.60				1.0	0.66	
Hf	6.6				6.7	3.8	

969

970 Table S3. Embayments and glass beads

Lunar sample #	74220				15421
MI #	2	4	4	6	1
host olivine diameter (μm)	245	330	330	glass bead	glass bead
host olivine Fo#	81	81	81		
embayment diameter (μm)	46	60	60	glass bead	glass bead
SiO_2 (wt%)	39.26	39.29		38.94	44.60
TiO_2	11.84	12.53		10.71	0.43
Al_2O_3	7.91	8.69		6.36	7.21
FeO	22.73	22.12		22.77	20.47
MnO	0.23	0.32		0.31	0.23
MgO	6.44	4.74		8.15	17.33
CaO	9.97	10.36		9.83	8.12
Na_2O	0.45	0.42		0.31	0.10
K_2O	0.09	0.10		0.05	0.01
P_2O_5	0.01			0.03	0.01
H_2O (ppm)	8.4	10.1	10.6	11.8	10.1
F	7.4	10.9	9.5	8.5	2.3
S	363	430	354	307	93
Cl	0.107	0.31	0.30	0.149	0.087
Sr	295	239		216	26
Y	61	51		52	8.4
Zr	239	201		199	21
Nb	17.3	14.9		14.5	1.33
Ba	104	86		72	13.9
La	8.3	8.1		6.9	1.54
Ce	26	21		21	3.1
Pr	4.2	3.3		3.7	0.41
Nd	23	21		21	2.3
Sm	10.2	7.9		7.4	1.16
Eu	2.1	0.98		2.9	0.74
Gd	12.0	9.5		9.3	1.18
Tb	3.0	2.8		2.6	0.22
Dy	12.4	10.8		10.7	1.12
Ho	1.99	2.0		2.0	0.173
Er	6.7	6.3		5.9	1.07
Tm	0.85	0.69		0.56	0.15
Yb	5.8	5.6		4.4	1.13
Lu	0.95	1.1		0.93	0.17
Hf	7.3	8.2		6.8	0.33

971

972

973 Table S4. Crystalline melt inclusions

Lunar sample #	10020								15016
MI #	10	10	11a	11a	11a	12	13a	13b	2
host olivine diameter (μm)	267	267	188	188	188	285	311	311	452
host olivine Fo#	71	71	69	69	69	71	71	71	54
inclusion diameter (μm)	30	30	14	14	14	15	86	88	43
SiO_2 (wt%)	48.24	54.86	55.12			54.65	53.88	53.61	57.54
TiO_2	1.99	5.35	3.03			4.66	3.33	2.80	2.33
Al_2O_3	26.07	10.04	14.22			9.42	17.25	16.46	15.48
FeO	3.41	7.72	5.27			7.96	7.25	7.07	8.39
MnO	0.12	0.13	0.08			0.10	0.09	0.14	0.06
MgO	1.00	2.26	1.60			3.51	1.41	1.73	2.69
CaO	19.24	18.52	19.83			19.41	15.54	17.46	14.07
Na_2O	0.45	0.18	0.58			0.58	0.60	0.34	0.89
K_2O	0.45	1.04	0.12			0.09	0.11	0.10	0.28
P_2O_5	0.10	0.19	0.20			0.20	0.03	0.04	0.09
H_2O (ppm)	116	8.8		82	342	110	2.4	65	17.9
F	307	55	83	18.6	106	84	45	51	96
S	874	127	93	27	247	109	350	631	387
Cl	4.7	0.96	3.2	0.65	4.2	8.2	4.8	8.2	4.1
Sr	164					163	193	211	134
Y	96					123	79	130	45
Zr	285					339	202	329	154
Nb	19.7					21	15.0	20.0	8.5
Ba	88					97	96	112	75
La	11.1					10.6	8.8	12.8	7.1
Ce	30					34	28	39.6	21
Pr	6.0					6.7	4.2	6.9	4.7
Nd	29					33	24	38	15.3
Sm	8.5					13.1	9.9	15.3	6.5
Eu	2.3					3.9		1.91	2.1
Gd	11.5					15.5	13.8	22	6.7
Tb	2.8					2.9	3.8	4.3	1.26
Dy	15.5					21	16.3	25	8.6
Ho	5.0					6.1	3.0	5.0	2.1
Er	8.9					12.2	9.7	14.9	4.1
Tm	0.97					2.2	1.2	2.0	1.0
Yb	10.2					14.9	9.1	13.8	3.7
Lu	1.1					1.3	1.5	2.6	0.69
Hf	8.9					8.7	6.7	14	6.3

974

975

976 Table S4.

Lunar sample #	12008							12040				
MI #	5	6a	6b	7	8a	8b	8c	1	2	3a	3b	3c
host oliv dia (μm)	416	150	150	514	258	258	258	487	564	661	661	661
host olivine Fo#	76	67	67	69	68	68	68	53	56	63	63	63
MI dia (μm)	35	18	29	45	21	33	21	66	32	27	32	21
SiO_2 (wt%)	49.16	49.33	51.94	63.75	46.61	46.16	47.26	57.91	57.55	62.64	64.57	66.24
TiO_2	5.82	4.31	4.44	1.83	5.99	6.25	4.99	1.83	1.79	1.79	0.54	1.46
Al_2O_3	14.81	13.80	14.31	14.19	13.81	13.48	14.77	14.37	14.96	17.52	21.55	13.95
FeO	10.14	10.21	12.46	6.02	11.67	13.45	10.97	7.38	8.71	4.25	2.15	6.07
MnO	0.20	0.15	0.16	0.10	0.15	0.21	0.15	0.09	0.08	0.08	0.01	0.02
MgO	3.57	3.30	2.83	3.27	3.12	3.60	2.71	3.22	2.25	2.56	0.70	4.55
CaO	15.66	16.28	15.45	12.77	15.28	14.11	16.14	14.85	16.57	12.08	12.21	7.51
Na_2O	0.41	0.31	0.41	0.55	0.43	0.46	0.32	0.38	0.21	0.70	0.78	0.39
K_2O	0.09	0.11	0.09	0.10	0.11	0.10	0.07	0.05	0.12	0.14	0.13	
P_2O_5	0.21	0.11	0.10	0.08	0.13	0.06	0.11	0.07	0.17	0.13	0.20	0.07
Cr_2O_3	0.20	0.15		0.16	0.14	0.19	0.13					
H_2O (ppm)	5.3	29	36	22	40	32	25	9.4	33	5.8	7.4	29
F	70	87	58	131	50	63	68	180	297	20	126	440
S	1394	942	1667	180	1623	1319	1871	331	386	22	125	77
Cl	6.2	4.5	2.8	5.7	2.7	2.7	3.8	1.89	4.1	0.21	3.8	2.0
Sr			161		169			98	127	80	133	
Y			61		63			78	79	42	41	
Zr			153		161			168	138	118	132	
Nb			7.4		6.5			6.4	9.2	6.4	9.7	
Ba			64.5		59			73	81	32	90	
La			7.9		7.4			6.7	9.5	4.5	9.0	
Ce			23		23			21	23.7	16.0	19.3	
Pr			4.0		4.2			4.3	3.6	2.8	3.1	
Nd			18.2		21			18.1	18.6	13.5	12.5	
Sm			7.2		8.5			8.0	6.8	5.2	4.3	
Eu			1.0					2.0			0.17	
Gd			8.6		8.7			9.1	10.1	6.4	7.5	
Tb			2.0		2.0			1.87	3.1	1.46	1.10	
Dy			11.6		11.3			13.4	13.9	8.5	7.2	
Ho			2.3		3.3			2.9	2.9	1.57	2.1	
Er			7.3		7.4			8.5	8.1	4.2	4.4	
Tm			1.4		1.1			1.4	1.4	0.96	1.2	
Yb			7.7		8.3			9.2	6.8	4.7	3.8	
Lu			0.97		1.1			1.0	1.2	0.67	0.29	
Hf			4.3		5.1			3.7	4.4	2.7	6.8	

977

978

Table S4.

Lunar sample #	15647					74235				
MI #	3	4a	4b	4c	4d	1a	1b	1c	2a	2b
host olivine diameter (μm)	369	853	853	853	853	258	258	258	296	296
host olivine Fo#	49	57	57	57	57	71	71	71	71	71
inclusion diameter (μm)	33	45	27	45	60	48	22	10	37	18
SiO_2 (wt%)	57.86	55.61	58.68	56.02	63.45	40.93	45.01	35.78	43.87	37.15
TiO_2	2.18	2.29	2.61	2.77	1.59	14.43	8.88	21.56	7.24	14.15
Al_2O_3	13.66	14.56	14.63	11.79	16.68	11.46	12.94	9.81	10.88	13.93
FeO	9.33	9.39	6.92	7.96	4.68	16.55	13.84	19.77	18.16	19.35
MnO	0.13	0.13	0.04	0.12	0.03	0.24	0.19	0.31	0.25	0.29
MgO	2.64	3.48	2.45	4.90	1.13	3.47	4.00	2.86	9.80	8.77
CaO	13.33	13.49	13.90	15.81	12.20	12.38	13.89	11.49	9.16	9.86
Na_2O	0.58	0.63	0.51	0.32	0.56	0.65	0.71	0.50	0.70	0.40
K_2O	0.14	0.04	0.10	0.04	0.17	0.12	0.12	0.09	0.12	0.07
P_2O_5	0.08	0.19	0.06	0.08	0.19	0.10	0.07	0.01	0.06	0.07
Cr_2O_3	0.06	1.00	0.87	0.45			0.41		0.33	0.43
H_2O (ppm)	9.8	12.1	6.7	40	6.6	25	38		57	
F	254	72	55	84	60	27	103	618	95	
S	326	132	313	313	349	225	1208	652	671	
Cl	10.6	3.2	3.4	6.3	3.4	1.91	5.0	23	3.3	
Sr	180	172	99	129	208	125	146	114	104	
Y	29	75	35	28	55	67	87	60	88	
Zr	112	271	116	114	280	202	245	163	236	
Nb	8.3	19.5	5.9	9.4	31	21	21	17.6	13.3	
Ba	105	116	49	59	145	62	76	53	46	
La	7.2	26	5.7	6.7	13.9	5.6	6.3	5.4	6.1	
Ce	18.8	73	15.9	17.1	36	16.3	19.1	15.6	16.2	
Pr	2.7	11.0	2.8	3.0	5.5	3.7	4.1	3.2	3.8	
Nd	13.8	48	13.7	13.2	27	22	24	16.4	21	
Sm	4.6	12.5	6.4	5.1	11.0	11.3	10.7	6.0	11.0	
Eu	1.1	0.81	0.077	0.48		0.19	1.7	1.9	0.26	
Gd	4.6	12.2	3.4	4.5	8.7	9.4	11.4	8.2	11.0	
Tb	0.89	1.83	0.98	0.92	1.60	1.87	1.99	1.79	1.82	
Dy	5.3	12.4	5.6	6.1	10.5	12.1	14.8	9.2	15.7	
Ho	1.13	3.6	1.33	1.38	3.2	3.9	4.1	2.3	3.8	
Er	2.6	6.3	2.7	2.6	6.3	7.1	10.0	6.6	8.4	
Tm	0.57	1.1	0.13	0.36	1.1	1.6	1.6	0.96	1.9	
Yb	2.9	5.3	3.4	2.2	7.2	10.7	11.2	7.6	9.6	
Lu	0.31	0.43	0.58	0.39	0.77	1.4	1.0	1.2	1.1	
Hf	4.9	5.2		3.4	14	4.2	7.4	9.5	7.3	